Universidade de São Paulo

Biblioteca Digital da Produção Intelectual - BDPI

Departamento de Física e Ciência Interdisciplinar - IFSC/FCI   Artigos e Materiais de Revistas Científicas - IFSC/FCI

2012-11

Mixed network former effect in ion-conducting Alkali borophosphate glasses: structure/property correlations in the system '['M IND. 2'O] IND. 1/3''['('B IND. 2''O IND. 3') IND. x''('P IND. 2''O IND. 5') IND. 1-x'] IND. 2/3' (M = 'LI', K, 'CS')

Mixed Network Former Effect in Ion-Conducting Alkali Borophosphate Glasses: Structure/Property Correlations in the System $[M_2O]_{1/3}[(B_2O_3)_x(P_2O_5)_{1-x}]_{2/3}$ (M = Li, K, Cs)

Dirk Larink and Hellmut Eckert*

Institut für Physikalische Chemie, Westfälische Wilhelms-Universität Münster, Corrensstrasse 30, 48149 Münster, Germany

Malinda Reichert and Steve W. Martin*

Department of Materials Science and Engineering, Iowa State University of Science & Technology, 2200 Hoover Hall, Ames, Iowa 50010, United States

Ⓢ Supporting Information

ABSTRACT: Glasses in the system $[M_2O]_{1/3}[(B_2O_3)_x(P_2O_5)_{1-x}]_{2/3}$ (M = Li, K, Cs) $(0.0 \leq x \leq 1.0)$ were prepared by standard melt-quenching procedures, and their physical properties were characterized by thermal analysis, density measurements, and impedance spectroscopy. Their atomic level structures were comprehensively characterized by Raman spectroscopy, by X-ray photoelectron spectroscopy (XPS), and by [11]B, ^{31}P, and [7]Li as well as [133]Cs high resolution solid state magic-angle-spinning (MAS) NMR techniques. ^{31}P MAS NMR peak assignments were aided by the presence or absence of homonuclear indirect [31]P−[31]P spin−spin interactions, "J-coupling", as detected via refocused INADEQUATE techniques. Consistent speciations of the phosphate and borate network former components in terms of the various P^n_{mB} and B^n_{mP} units, where n is the number of bridging oxygens (BOs) and m is

the number of B or P units bonded to P or B, respectively, present in these glasses were derived from ^{11}B MAS NMR, combined with both ^{31}P MAS NMR and XPS line shape analyses, constrained by charge and mass balance considerations. The speciation of the BO species in the glassy network was quantified both by O 1s XPS and [11]B{[31]P} rotational echo double resonance spectroscopy. Both experiments indicate a strong preference of heteroatomic B−O−P over homoatomic P−O−P and B−O−B linkages to the extent that close to the maximum number of possible B^4−O−P linkages is formed. Further, the structural speciations of the borate and phosphate species, together with bond valence (BV) analyses of the charge redistribution on the various structural units, indicate that the alkali network modifier oxide is not proportionally shared between the two network former components B and P in these systems. Rather, the amounts and types of the various borate and phosphate species are found to be consistent with the negative charge brought in by the alkali modifier M_2O being distributed more toward the phosphate structural units which are suggested to attract a larger concentration of network modifier species than predicted by the bulk composition. The experimental results obtained from these studies help in understanding the strongly nonlinear compositional dependence of the glass transition temperature and the ionic conductivity in terms of detailed atomic-level structural information. The emerging structural principles appear to be general to all of the alkali borophosphate glass systems, with the type of alkali ion network modifier producing only minor variations.
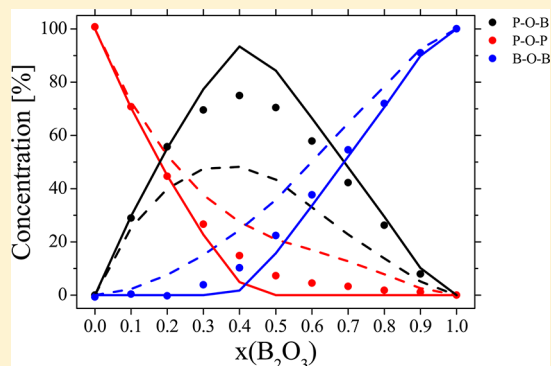
■ INTRODUCTION

Ternary alkali borophosphate glasses are known for their remarkable physical and chemical stabilities, combined with enhanced ionic conductivities, which makes their use as solid electrolytes greatly preferable to that of pure binary alkali borate or phosphate analogues.[1−10] The strongly nonlinear dependences of their physical properties on the composition (mixed glass former effect, MGFE) make these glasses ideal model systems for the fundamental study of structure−property correlations. To this end, numerous experimental methods, including vibrational spectroscopy, X-ray photoelectron spectroscopy (XPS), and

advanced solid state nuclear magnetic resonance techniques, have been recently adapted and applied to various compositional sections of the ternary $Na_2O−B_2O_3−P_2O_5$ system.[11−16] In addition, the structural speciations of various other borophosphate glass systems have been studied by NMR.[17−20] These studies have resulted in detailed quantitative speciations of the short-range order (SRO) and intermediate-range order (IRO) of these glasses in terms of the
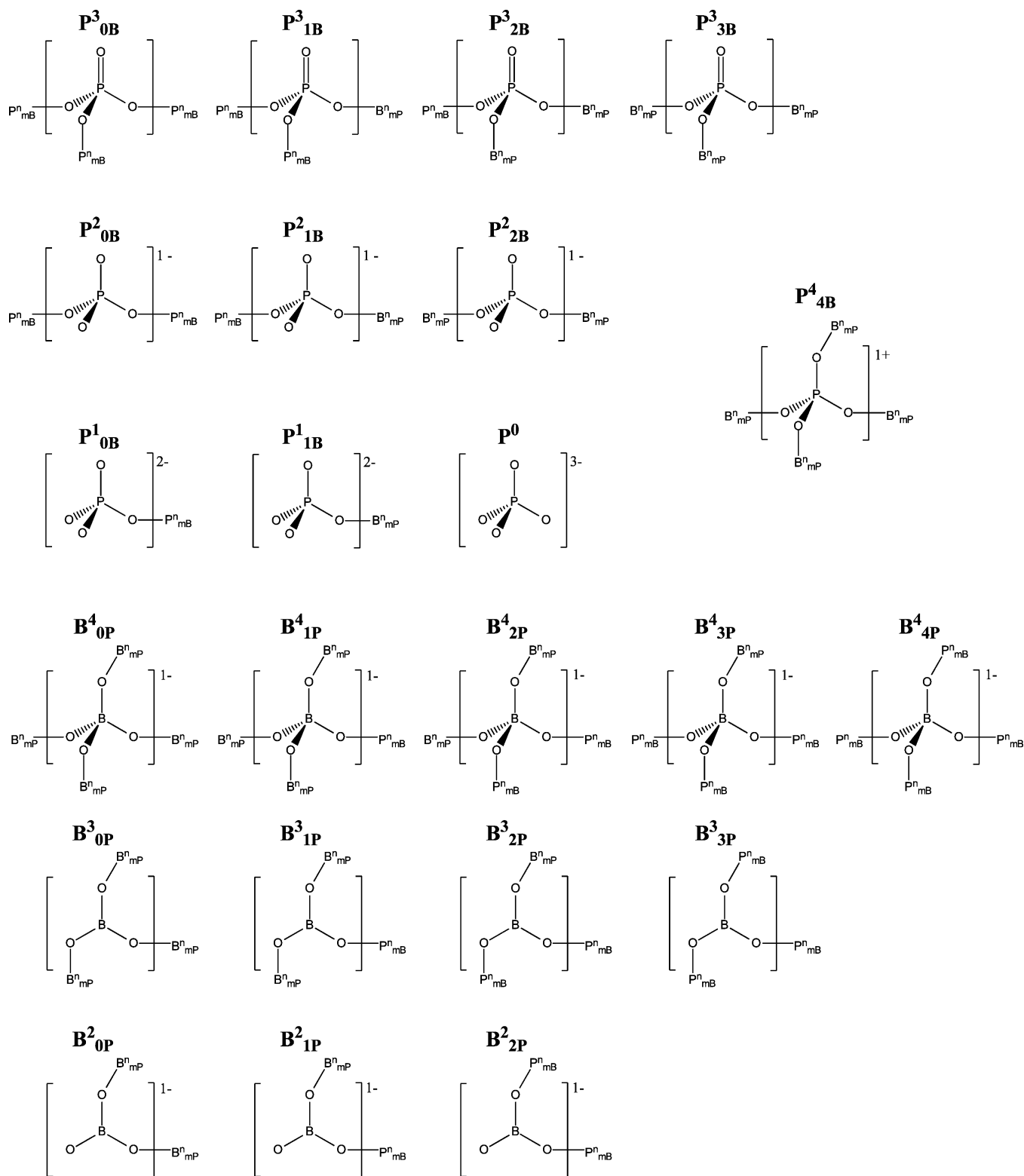
Figure 1. Local environments and connectivities present in glasses of the systems $[M_2O]_{1/3}[(B_2O_3)_x(P_2O_5)_{1-x}]_{2/3}$ (M = Li, K, Cs). As discussed further below, P=O double bonds displayed for P^3_{mB} units ($m > 0$) are only partial and charges are considered formal charges only.

distinct structural units differentiating the first and second coordination spheres. Figure 1 summarizes the various borate and phosphate SRO structural units and introduces the P^n_{mB} and B^n_{mP} nomenclature used, where n denotes the number of bridging oxygen (BO) atoms and m ($\leq n$) specifies the number of heteroatomic linkages per network former species.

For mixed network former glass systems in which the ionic conductivity is the focus, it is most desirable to keep the variations of the mobile ion concentrations as small as possible and to vary the ratio of the two network former species present.[11,12,15,16,18,20] Furthermore, the influence of cation size and type on the magnitude of the MGFE and the different structural aspects of

Table 1. Theoretically Expected and Analytical Compositions (in atom %) for the Glass Systems Studied

					analytical composition/atom %					
	batch composition/atom %				K system			Cs system		
	M	B	P	O	K	P	O	Cs	P	O
$x = 0.0$	11.8	0.0	23.5	64.7	11.6	24.0	64.4	12.6	24.9	62.5
$x = 0.1$	12.1	2.4	21.7	63.9	11.5	22.7	63.3	12.3	22.9	62.4
$x = 0.2$	12.4	4.9	19.8	63.0	10.4	19.6	65.0	9.9	19.3	65.9
$x = 0.3$	12.7	7.6	17.7	62.0	12.8	19.5	60.1	11.2	18.1	63.1
$x = 0.4$	13.0	10.4	15.6	61.0	12.7	17.3	59.6	13.1	16.7	59.8
$x = 0.5$	13.3	13.3	13.3	60.0	13.4	14.9	58.3	10.8	13.5	62.4
$x = 0.6$	13.7	16.4	11.0	58.9	13.3	12.1	58.2	11.6	11.3	60.6
$x = 0.7$	14.1	19.7	8.5	57.8	13.7	9.5	57.1	11.5	8.2	60.5
$x = 0.8$	14.5	23.2	5.8	56.5	14.9	6.7	55.2	13.5	6.3	57.1
$x = 0.9$	14.9	26.9	3.0	55.2	14.8	3.5	54.9	15.1	3.3	54.8
$x = 1.0$	15.4	30.8	0.0	53.9	14.5	0.0	54.8	14.3	0.0	54.8

these glasses is not yet clear and has been little studied. While lithium[20] and silver[18] borophosphate glasses have been examined, these studies were done on samples with much higher modifier ion contents. The present contribution reports the results of a systematic structural study of glasses in the system $[M_2O]_{1/3}[(B_2O_3)_x(P_2O_5)_{1-x}]_{2/3}$, with M = Li, K, and Cs. While the compositions of these glasses bear close resemblance to the analogous Na-based system studied in refs 15 and 16, the present study focuses explicitly on the quantitative structural aspects. On the basis of an encompassing spectroscopic strategy involving Raman, XPS, and complementary advanced solid state NMR spectroscopic techniques, we develop a comprehensive structural model describing the composition, x, dependence of the various SRO structures found in these ternary glasses, the polyhedral connectivities, and the distribution of the alkali network modifier between the two network forming components in these mixed glass former systems.

EXPERIMENTAL SECTION

Glasses were prepared in 15 g batches by traditional melt cooling methods in an open system. The starting materials Li_2CO_3 (Fisher Scientific, 99.8%), K_2CO_3 (Fisher Scientific, 99.9%), Cs_2CO_3 (CERAC, 99.996%), H_3BO_3 (Fisher Scientific, 99.7%), and $(NH_4)_2HPO_4$ (Fisher Scientific, 99.7%) were dried at 423 K for at least 48 h in a drying oven. The materials were ground together in an agate mortar and heated within a Pt crucible to 1200−1400 K for ~1 h and subsequently cooled to room temperature by removal from the furnace. Mass losses were as expected due the decomposition of the starting materials evolving NH_3, H_2O, and CO_2 gases. Excess mass losses due to evaporation of the formed melt were regularly checked and were never found to exceed 2 wt %. Samples were introduced into a nitrogen-filled glovebox, where they were remelted at 1200−1400 K for periods of approximately 10 min and subsequently poured into brass molds that were preheated to a temperature about 50 K below the respective glass transition temperature, T_g. Subsequently, the samples were annealed within the copper molds at ~5 K below T_g and then cooled to room temperature at a rate of 0.5 K/min. All sample handling and long-term storage were done in the dry nitrogen atmosphere, with H_2O and O_2 contents < 5 ppm, of the glovebox. Densities were measured using the Archimedes method where previously dried kerosene was used as the immersion fluid.

For the potassium- and cesium-based glasses, sample compositions were measured by energy dispersive X-ray fluorescence spectroscopy (EDX) on cylindrical samples with 2−3 mm thickness. Before these measurements, samples were polished to

create fresh surfaces and, subsequently, gold electrodes were sputtered on one side of the disk-shaped samples inside the glovebox to improve the electrical contact of the samples with the sample holder. As illustrated in Table 1 and Figure S1 (Supporting Information), the analytically determined compositions were found to be in excellent agreement with batch compositions.

T_g (onset points) were measured with a Perkin Elmer Pyris Diamond differential scanning calorimeter on ~10 mg samples at a heating rate of 10 K/min. The T_g's were determined on replicate heating scans where the glass had been previously cooled at 10 K/min.

Ionic conductivity measurements were conducted using a Novocontrol Concept 80 impedance spectrometer. Samples were measured over the frequency range $10^{-2}−10^6$ Hz, between 200 and 550 K, at an applied voltage of 20 mV on samples of 1−2 mm thickness (Ø = 20 mm). To improve the contact between the glass and the electrodes, the surfaces were covered with a thin layer of gold by rf magnetron sputtering inside the glovebox. During the isothermal frequency sweeps of the complex impedance, the temperature of the conductivity cell was controlled within ±0.2 K and samples were equilibrated for 30 min at each temperature. The dc ionic conductivities were extracted from Nyquist plots by extrapolating the imaginary part of the impedance, Z'', to the intercept along the real part of the complex impedance, Z', axis.

Raman spectra were collected using a Renishaw inVia spectrometer using an argon laser at 488 nm, and Fourier transform infrared (FT-IR) absorption measurements were collected using a Bruker IFS 66v/s spectrometer on CsI pellets containing 1−3 wt % glass.

XPS measurements on the K-based glasses were conducted on a Kratos Axis Ultra spectrometer using Al Kα (1486.6 eV) as the radiation source and a charge neutralizer device to avoid surface charging. The acceleration voltage was 12 kV, and the emission current was 10 mA. High-resolution spectra were measured with pass energies of 20 eV. All the measurements were done on samples freshly ground in an argon-filled glovebox. The powders were pressed into copper sample holders and immediately introduced into the ultrahigh vacuum atmosphere (10^{-12} bar) of the spectrometer. Data were analyzed using the CasaXPS software.

All NMR experiments were carried out at ambient temperature on Bruker DSX-400 and DSX-500 and Bruker Avance 300 and 600 spectrometers with magic-angle-spinning probes of 2.5 or 4 mm diameter. Spectral deconvolution of the resulting NMR spectra was performed using the DMFIT software package.[22]

Table 2. Glass Transition Temperatures T_g, Densities ρ, and Molar Volumes V_m for the $[M_2O]_{1/3}[(B_2O_3)_x(P_2O_5)_{1-x}]_{2/3}$ Systems Studied

	Li system			K system			Cs system		
	T_g ($\pm$5)/K	ρ ($\pm$0.02)/ (g/cm^3)	V_m ($\pm$0.2)/ (cm^3/mol)	T_g ($\pm$5)/K	ρ ($\pm$0.02)/ (g/cm^3)	V_m ($\pm$0.2)/ (cm^3/mol)	T_g ($\pm$5)/K	ρ ($\pm$0.02)/ (g/cm^3)	V_m ($\pm$0.2)/ (cm^3/mol)
$x = 0.0$	509	2.33	44.8	506	2.36	53.4	460	3.11	60.6
$x = 0.1$	597	2.34	42.7	533	2.40	50.5	503	3.15	58.3
$x = 0.2$	657	2.38	39.9	586	2.39	48.6	534	3.20	56.0
$x = 0.3$	690	2.43	37.1	648	2.44	45.8	624	3.25	53.6
$x = 0.4$	726	2.47	34.5	705	2.47	43.3	698	3.33	50.9
$x = 0.5$	732	2.45	32.9	724	2.47	41.3	703	3.39	48.6
$x = 0.6$	725	2.40	31.5	709	2.43	40.0	672	3.37	47.3
$x = 0.7$	727	2.33	30.4	697	2.38	38.8	656	3.36	46.1
$x = 0.8$	736	2.31	28.6	700	2.34	37.4	656	3.34	44.8
$x = 0.9$	756	2.28	26.8	710	2.32	35.7	682	3.40	42.8
$x = 1.0$	765	2.26	24.9	709	2.30	33.9	661	3.43	40.9

[11]B single pulse MAS experiments were carried out at 192.50 MHz using a 14.1 T magnet at spinning frequencies of 12.0 kHz. Typical acquisition parameters were pulse lengths of 0.5 μs (20° flip angle) and recycle delays of 5 s. Chemical shifts are reported relative to a CDCl$_3$ solution of BF$_3$·OEt$_2$. ^{31}P single pulse MAS NMR experiments were carried out at 121.44 MHz using a 7.1 T magnet at sample spinning frequencies of 14.0 kHz. Typical acquisition parameters were pulse lengths of 3.0 μs (90° flip angle) and recycle delays of 300 s. Chemical shifts are reported relative to 85% H$_3$PO$_4$. ^{7}Li MAS NMR spectra were recorded at 233.18 MHz in a 4 mm probe on the Bruker Avance 600 spectrometer; 20° pulses of 0.5 μs length and relaxation delays of 30 s were used to collect the spectra. Chemical shifts are referenced against a 1 M aqueous solution of LiCl. [133]Cs MAS NMR spectra were recorded as rotor synchronized spin echos, at 65.59 MHz, using the Bruker DSX-500 spectrometer and a 2.5 mm probe. Samples were rotated at a spinning speed of 30.0 kHz. The 90° and 180° pulse lengths were 2.5 and 5.0 μs, respectively, and a relaxation delay of 5 s was used. Chemical shifts are reported relative to 1 M aqueous CsCl solution.

The connectivity between different types of phosphorus units was further probed by one-dimensional refocused INADEQUATE experiments.[23] This technique relies on double quantum filtering, based on homonuclear J-coupling, to yield correlation peaks between nuclei engaged in P−O−P linkages. In these experiments, the signals from isolated ^{31}P nuclei are suppressed because the absence of J-coupling in them precludes the formation of double quantum coherences. All refocused INADEQUATE experiments were done on the Bruker Avance 300 spectrometer with a 4 mm probe using spinning frequencies of 14.0 kHz, π/2 pulse lengths near 3.0 μs, and a fixed t_1 increment of 71.4 μs. Sixty-four to 2368 scans were taken. In all of the experiments, the double quantum coherence buildup time $2T$ was set to around 6.25 ms, which is significantly shorter than the value of 50 ms corresponding to $1/2J$ expected for maximum double quantum coherence buildup.

Dipolar interactions between [11]B and ^{31}P were probed on representative samples by [11]B{[31]P} rotational echo double resonance (REDOR) spectroscopy.[24] These measurements were conducted using the Bruker DSX-400 spectrometer with a 4 mm probe at 9.4 T and spinning frequencies of 8.0, 10.0, and 12.0 kHz. Typical π pulse lengths were 8.0 and 9.0 μs for [11]B and ^{31}P, respectively. [11]B{[31]P} REDOR data were acquired using 16 accumulated scans with relaxation delays of 5 s between scans. Following previously established procedures,[25,26] dipolar second moments, M_2([11]B{[31]P}), could be

extracted from the initial part of the [11]B{[31]P} REDOR curves ($\Delta S/S_0 \leq 0.20$) using the expression[26]

$$\frac{\Delta S}{S_0} = \frac{4}{3\pi^2}M_2^{SI}(NT_r)^2 \tag{1}$$

The compensation pulse scheme was used[26] and the π pulses on the ^{31}P decoupler channel were phase cycled following the XY4 scheme.[27] The experimental conditions were calibrated using parallel experiments on the previously measured reference material Na$_5$B$_2$P$_3$O$_{13}$.[28]

RESULTS, DATA ANALYSIS, AND INTERPRETATION

Bulk Properties. All the glasses were found to be homogeneous and transparent, exhibiting singular T_g's, and no other evidence for phase separation effects was observed. The T_g's are summarized in Table 2 together with bulk densities ρ and molar volumes V_m. Figure 2 illustrates the nonlinear composition dependences of all of these parameters. Figure 2c emphasizes the nonlinearity observed for V_m by calculating ΔV_m, the deviation from a linear composition dependence. This quantity shows a pronounced minimum near $x = 0.4−0.5$, indicating that the glass structure appears particularly dense and compact at this composition. Strongly nonlinear composition dependences are also seen for the T_g values. They increase steadily up to $x = 0.4$ and remain approximately constant at higher x values. Within the composition range $0.6 \leq x \leq 1.0$, a slight influence of the modifier cation type can be seen. For the lithium-based glasses, the T_g values tend to increase slightly with increasing x. For the potassium-based glasses the values stay more or less constant. Finally, for the cesium-based glasses a slight decrease is noted. Figure 3a plots the alkali ion concentrations, N_V, as a function of composition. In general, N_V is expected to increase monotonically with increasing x reflecting the higher atomic fraction of the alkali ions in the alkali borate (0.154) compared to the alkali phosphate end member (0.118). Nevertheless, Figure 3a shows a slight maximum for each of the glass series near $x = 0.4−0.5$. All of these observations point toward significant structural condensation caused by the interaction of the two network former species in this compositional range. The similarity in the composition dependence of these physical properties among the three different alkali borophosphate glasses suggests that the composition dependences of the various SRO groups in all three glass series are quite similar and suggests that the influence of the alkali cation type on the overall structural organization of these glasses is weak.
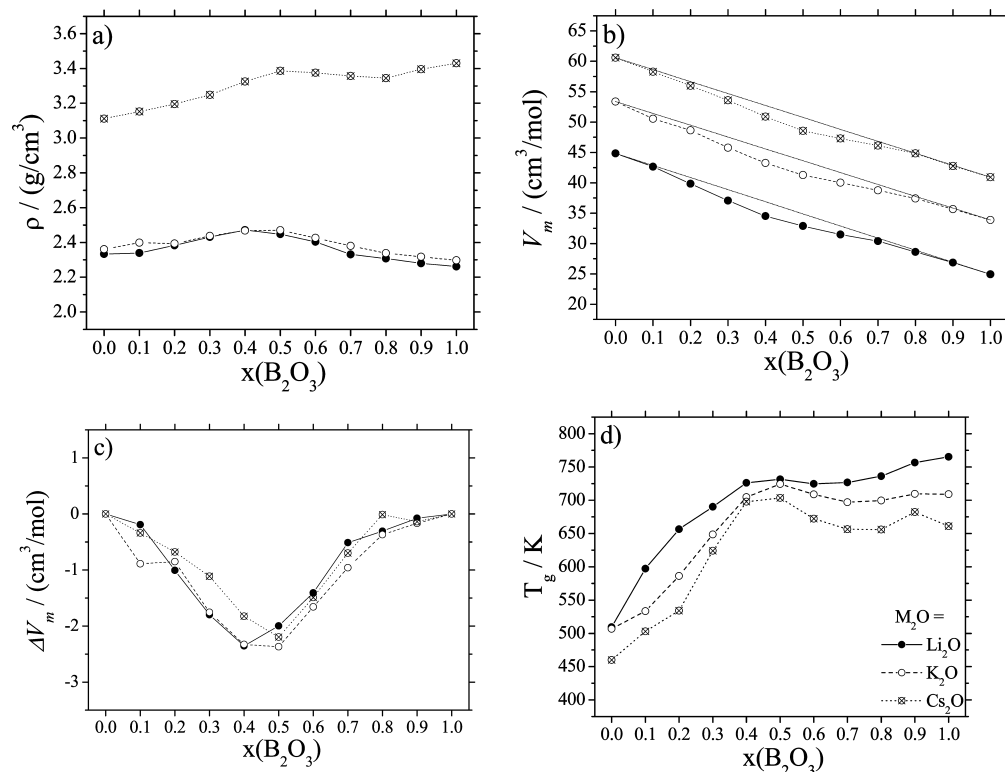
Figure 2. (a) Bulk densities ρ, (b) molar volumes V_m, (c) deviations of molar volumes from linear composition dependences, ΔV_m, and (d) glass transition temperatures T_g in glasses of the systems $[M_2O]_{1/3}[(B_2O_3)_x(P_2O_5)_{1-x}]_{2/3}$ (M = Li, K, Cs).

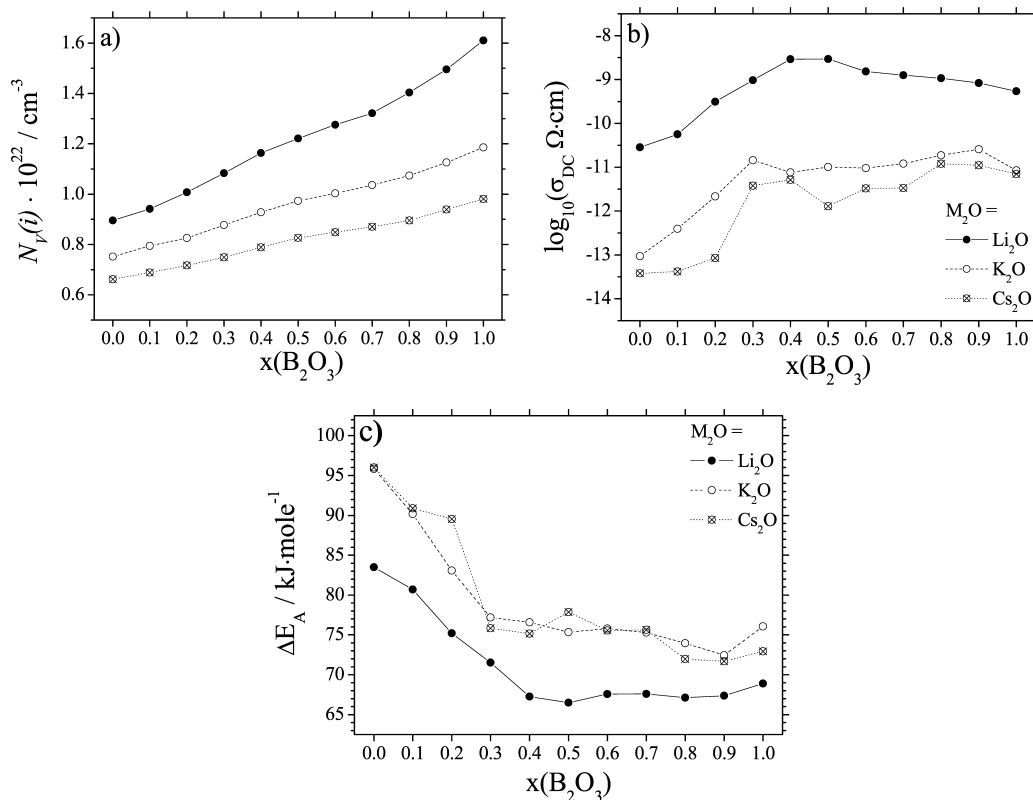**Figure 3.** (a) Ionic number densities $N_V(i)$, (b) dc ionic conductivities at 300 K, and (c) activation energies ΔE_A derived from temperature dependent dc conductivity measurements of glasses in the systems $[M_2O]_{1/3}[(B_2O_3)_x(P_2O_5)_{1-x}]_{2/3}$ (M = Li, K, Cs).

Figure 3b,c shows plots of the room temperature ionic conductivities and their corresponding activation energies as a function of composition, x. As previously observed for compositionally related glasses in the sodium borophosphate system,[11,12]
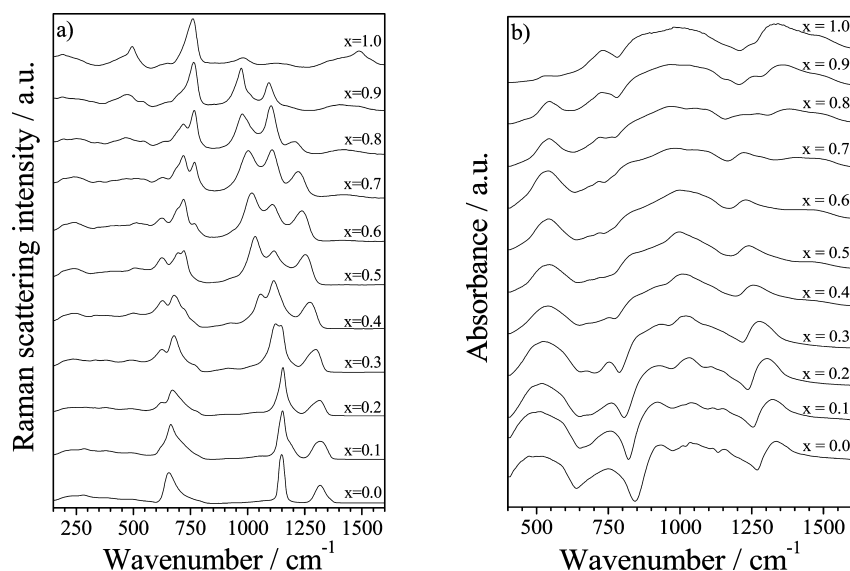
Figure 4. (a) Raman spectra of glasses in the system $[K_2O]_{1/3}[(B_2O_3)_x(P_2O_5)_{1-x}]_{2/3}$. (b) FT-IR absorption spectra of glasses in the system $[K_2O]_{1/3}[(B_2O_3)_x(P_2O_5)_{1-x}]_{2/3}$. The individual components of these stack plots have been internally normalized to a constant maximum intensity and are shown with a constant vertical offset with respect to each other.

a significant increase in ionic conductivity is observed up to $x \sim 0.5$, whereas at higher borate contents the conductivities are only weakly dependent on composition. As expected, the conductivities increase in the order Cs → K → Li borophosphate glasses, presumably reflecting the effect of ion size. Indeed, one of the authors has studied the effect of the alkali cation size on the alkali ion conductivity in detail in previous work, and the behavior observed here is very similar to that observed for other alkali ion conducting glasses.[29]

Raman and FT-IR Spectra. Figure 4a shows the Raman spectra of the K-containing glasses; spectral results for the lithium and cesium glasses were found to be very similar (see Figure S2 in the Supporting Information). The binary phosphate glasses show Raman spectra in excellent agreement with the literature.[30] In the potassium phosphate glass ($x = 0.0$), the three major bands observed at 655, 1150, and 1317 cm^{-1} can be assigned to the symmetric P—O—P stretching mode, the symmetric PO$_2$ stretching mode associated with the nonbridging oxygen (NBO) atoms of metaphosphate groups (P^2 units), and the symmetric P=O stretching mode of the P^3 units, respectively. The pure potassium borate glass ($x = 1.0$) shows five Raman scattering maxima near 495, 638, 760, 980, 1130, and 1489 cm^{-1}. Following the assignments of Bril,[31] the 760 cm^{-1} band is assigned to a symmetric breathing mode of six-membered rings containing two B^3 units and one B^4 unit (a so-called triborate unit) and the band at 1489 cm^{-1} is assigned to the B—O stretching mode of B^2 units which bears a NBO species. The assignments of the other bands are less certain. Based on the work of Konijendijk,[32] the bands at 495 and 980 cm^{-1} may be assigned to vibrations of the pentaborate group and the band at 1130 cm^{-1} is assigned to the vibration of the diborate units. Inspection of Figure 4a makes it clear that the Raman spectra of the mixed network former glasses cannot simply be viewed as superpositions of the spectra of the binary glasses; rather the formation of new structures is evidenced. As the x value increases from 0 to higher values, the band assigned to the P=O stretching mode of the P^3 units at 1317 cm^{-1} in the pure ultraphosphate glass shifts monotonically toward lower wavenumbers, down to 1250 cm^{-1}. We attribute this shift to a successive weakening of

the double bond character of the P^3 units, associated with their successive involvement in P—O—B linkages. Its presence in the spectra up to $x = 0.8$ shows that the P^3 group contributes to the structures of these glasses for almost all compositions containing phosphorus. As discussed further below, the wavenumber shift is consistent with the increasing partial anionic character leading to a weakening of the NBO atoms, as also indicated in Figure 1. Furthermore, the band at 1150 cm^{-1}, the symmetric PO$_2$ stretching mode, successively weakens in intensity and disappears at $x = 0.4$. Above $x = 0.2$, two new bands at 1122 and 1057 cm^{-1} gradually appear in the spectra and also shift continuously toward lower wavenumbers with increasing x. On the basis of this composition dependence and in conjunction with the NMR spectra to be discussed below, we can assign these bands to P$^2_{1B}$ and P$^2_{2B}$ units, respectively, reflecting the successive formation of P—O—B linkages. In the $x = 0.9$ sample, the latter band has shifted to ~ 971 cm^{-1}. On the basis of the NMR evidence discussed further below, we attribute this band to P^1 units at this composition. Remarkable changes are also observed in the region from 600 to 760 cm^{-1} and reflect the successive conversion of P—O—P linkages into P—O—B linkages with increasing x. The mode at 760 cm^{-1} assignable to triborate groups, Na$_2$O:3B$_2$O$_3$ = NaB$_3$O$_5$, is observable above $x = 0.6$ and suggests the formation of six-membered rings linking 3- and 4-fold boron atoms.

Finally, it appears that the Raman scattering cross section of the phosphate structural groups is significantly greater than that of the borate structural groups. While the Raman spectral features in the pure borate glass can be scaled to the same intensity level as the much more intense spectral features of the phosphate groups in the pure and mixed glasses, these features are difficult to discern in the mixed glasses, especially for the low borate content glasses where the spectral intensity is dominated by the phosphate structural groups. This makes using the Raman spectra to probe the borate structural groups in the $0 < x \leq 0.4$ region very difficult.

The FT-IR absorption spectra for the Li-based, K-based, and Cs-based glasses, Figure 4b and Figure S3 in the Supporting Information, show generally the same trends as observed in the Raman spectra, albeit with much less spectral fidelity because the
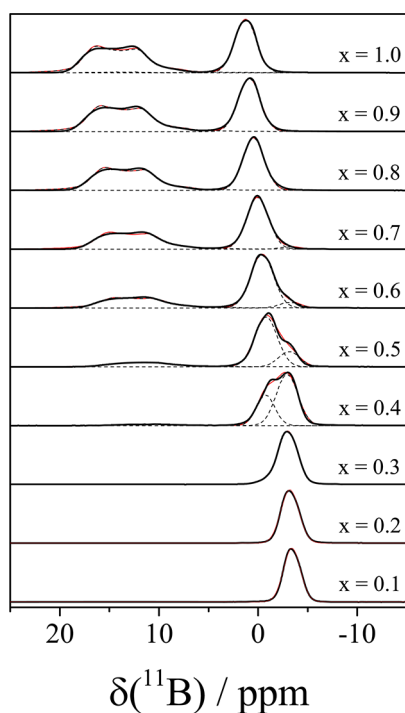
Figure 5. ^{11}B MAS NMR spectra of glasses in the system $[K_2O]_{1/3}$-$[(B_2O_3)_x(P_2O_5)_{1-x}]_{2/3}$. Included are line shape deconvolutions into individual spectroscopic components. The individual components of these stack plots have been internally normalized to a constant maximum intensity and are shown with a constant vertical offset with respect to each other.
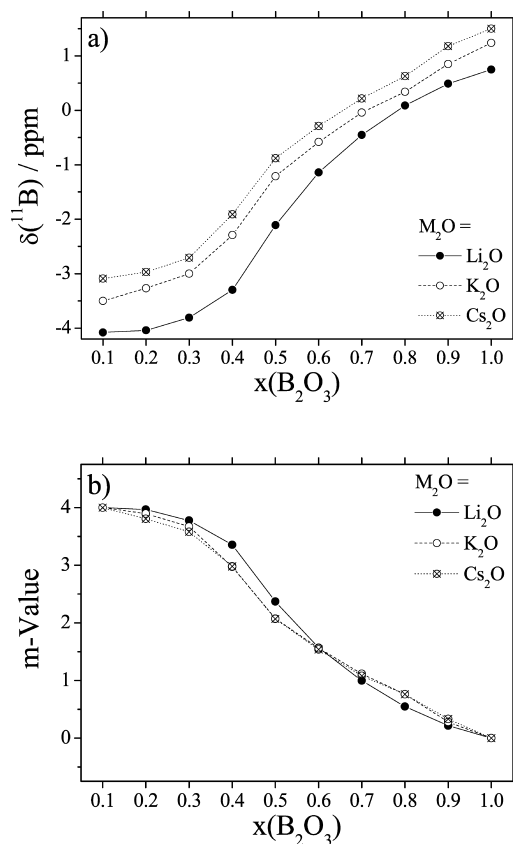

Figure 6. (a) Average isotropic chemical shifts measured for the B^4 resonances and (b) average values of m, the number of bridging bonds from B to P, deduced from these measurements in glasses of the systems $[M_2O]_{1/3}[(B_2O_3)_x(P_2O_5)_{1-x}]_{2/3}$ (M = Li, K, Cs).

IR absorption bands are more numerous and significantly broader than bands in the Raman spectra shown above, leading to significantly greater spectral overlap. However, some assignments can be made, and in the x = 0.0 sample, for example, the spectral features at 1430 and 1270 cm^{-1} are assigned to the symmetric P=O stretching vibration of P^3 units and the antisymmetric PO$_2$ stretching vibration of the P^2 units, respectively. With increasing x, these bands shift gradually toward lower wavenumbers, reflecting the effect of the P–O–B connectivity of this unit upon the vibrational wavenumber of the NBOs. Furthermore, bands observed near 850 and 640 cm^{-1} are assigned to stretching and torsional modes associated with the vibrational motion of the BO species. With increasing x, the 850 cm^{-1} band is strongly shifted toward lower wavenumbers, which can again be understood in terms of a successive replacement of P–O–P by P–O–B bridges. Also, a new band near 690 cm^{-1} appears in the IR spectra of glasses in the composition range $0.1 \leq x \leq 0.4$, whose assignment is uncertain at the present time. At the highest x values, $x \geq 0.8$, bands near 800 and 1200 cm^{-1} are assigned to B–O stretching modes associated with B^4 and B^3 units, respectively. It is noted that, as in the Raman spectra discussed above, borate vibrational modes are difficult to discern at lower boron contents due to the weaker IR absorption coefficients. Again, comparison of the spectra in Figure 4b with those of the Li- and Cs-based glasses (Figure S3 in the Supporting Information) reveals a striking similarity and indicates that the structural evolution observed in these borophosphate glasses with substituting one glass former, B_2O_3, with another, P_2O_5, are essentially independent of the alkali cation type.

High-Resolution ^{11}B MAS NMR and ^{11}B{^{31}P} REDOR Spectra. Figure 5 shows the ^{11}B MAS NMR spectra for the

compositional series for the K-based glasses; analogous data for the Li- and Cs-containing glasses are included in the Supporting Information, Figure S4. As in previously published ^{11}B MAS NMR spectra of other types of alkali and silver borophosphate glasses, three-coordinated boron species (B^3 and B^2 species) and four-coordinated boron species (B^4) are spectrally well separated. Up to x = 0.3, all of the boron atoms are observed to be four-coordinated and give rise to signals near −3.1, −3.4, and −4.1 ppm in the Li-, K-, and Cs-containing glasses, respectively. In agreement with previous studies, we assign this signal to B^4_{4P} units in all of the glasses. The systematic ^{11}B chemical differences observed between the Li, K, and Cs borophosphate glasses persist all the way up to the pure alkali borate glasses (Figure 6a), and we therefore attribute them to the effect of the differing cation charge densities.

As the boron content is increased beyond x = 0.3, increasing amounts of three-coordinated boron species are evidenced by the anisotropically broadened signal near 18 ppm. On the basis of their line shape parameters, in particular the small asymmetry parameter, we assign these borate species to neutral $BO_{3/2}$ (B^3) groups. It appears (see below) that negatively charged B^2 units only exist for the pure alkali borate glasses. Together with the appearance of the signal intensity for B^3 units in the spectra, the B^4 resonance splits into several components which reflect B^4_{mP} environments with different m values of ≤4. In principle, five distinct units may be expected, corresponding to B^4 atoms having zero, one, two, three, or four B–O–P linkages. In the spectra, however, maximally two distinct signal components are resolvable at each composition and a general shift toward higher

frequencies is observed as x is increased. As previously shown,[11] the average chemical shift measured for these chemically different B^4 species is linearly correlated with the average number m for the various different B^4_{mP} local environments. Using this correlation, we can deduce m for the B^4 species from the spectra shown in Figure 5 and Figure S4 in the Supporting Information. The results are illustrated in Figure 6b, while Figure 7 plots the
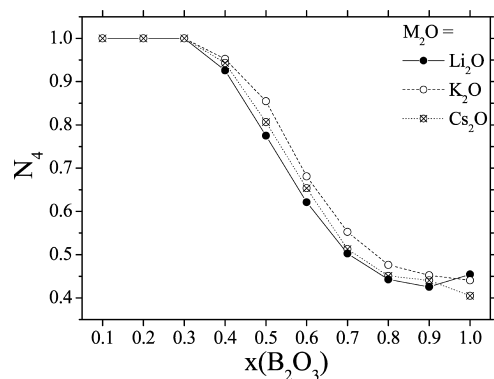

Figure 7. Fraction of the four-coordinated boron species N_4 in glasses of the systems $[M_2O]_{1/3}[(B_2O_3)_x(P_2O_5)_{1-x}]_{2/3}$ (M = Li, K, Cs).

total fraction N_4 of B^4 species as a function of x for all three systems. Again, the generally close similarity of the spectra for the three glass systems having different alkali counterions is striking. Small differences appear mostly with regard to the N_4 values, which tend to be slightly lower for the Li system than those for the K and Cs glasses, except for the binary alkali borate glasses, where the order is reversed. Subtle differences, albeit close to

experimental error limits, are also observed in the B^4_{mP} connectivity distributions, particularly in the composition range $0.4 \leq x \leq 0.7$. Table 3 and Tables S5 and S6 in the Supporting Information summarize the ^{11}B NMR fitting parameters for the K-, Li-, and Cs-based glasses, obtained in part on the basis of ^{11}B TQMAS NMR data (for representative spectra, see Supporting Information, Figure S7a−c). In agreement with the Raman and FT-IR results, it is found that asymmetric anionic B^2 units, i.e., $BO_{2/2}O^-$ groups, are only detected in the pure borate glasses, i.e., for $x = 1.0$; there appears to be no evidence for them in any of the ternary alkali borophosphate glasses.

Figure 8a summarizes typical results from the $^{11}B\{^{31}P\}$ REDOR NMR measurements. These data clearly illustrate the pronounced differences between the B^4 and the B^3 units with regard to the $^{11}B-^{31}P$ dipolar coupling strengths, in agreement with the observations made for alkali and silver borophosphate glass systems.[13,14,18,20,21] Dipolar second moments $M_2(^{11}B\{^{31}P\})$, obtained via eq 1, are summarized in Table 4 and plotted in Figure 8b for the B^4 units. As previously discussed, the numerical values express the extent of P−O−B connectivity, with a contribution of about 4×10^6 rad^2 s^{-2} per B−O−P linkage. Thus, the data illustrate the expected decrease of B−O−P connectivity from predominantly B^4_{4P} units at low x values, P_2O_5-rich glasses, to predominantly B^4_{0P} units at $x = 1.0$, B_2O_3-rich glasses, along with the decreasing P/B ratio. Assuming $m = 4$ for $x = 0.1$ and based on $m = 0$ for $x = 1.0$, estimates of m can be obtained from the measured M_2 values by interpolation (see Table 4). As illustrated by Figure 8c, these values are generally well correlated with those estimated from the average ^{11}B NMR chemical shifts of the B^4 species (Table 3). A systematic deviation occurs for samples in the concentration interval $0.5 \leq x \leq 0.8$, where the average value of m estimated from the REDOR results is higher than that based

Table 3. Deconvolution of the ^{11}B MAS NMR Spectra of Glasses in the System $[K_2O]_{1/3}[(B_2O_3)_x(P_2O_5)_{1-x}]_{2/3}$[a]

	B^n	δ_{CS}^{iso} (± 0.1)/ppm	G/L[b] (± 0.1)	LB[c] (± 0.5)/ppm	C_Q (± 0.05)/MHz	η_Q (± 0.1)	m value	area fract. (± 2)/%
$x = 0.1$	$B^4(1)$	−3.4	1.0	2.0	−	−	4.0	100
$x = 0.2$	$B^4(1)$	−3.2	1.0	2.1	−	−	3.8	100
$x = 0.3$	$B^4(1)$	−3.0	1.0	2.3	−	−	3.6	94
	$B^4(2)$	−0.8	1.0	2.2			3.6	6
$x = 0.4$	$B^4(1)$	−2.9	1.0	2.6	−	−	3.0	64
	$B^4(2)$	−0.8	1.0	2.2	−	−	3.0	31
	B^3	15.2	−	−	2.6	0.2	−	5
$x = 0.5$	$B^4(1)$	−3.1	1.0	2.5	−	−	2.1	19
	$B^4(2)$	−0.8	1.0	2.7	−	−		66
	B^3	16.1	−	−	2.6	0.2	−	15
$x = 0.6$	$B^4(1)$	−3.2	1.0	2.5	−	−	1.5	7
	$B^4(2)$	−0.4	1.0	2.7	−	−	1.5	61
	B^3	17.0	−	−	2.6	0.2	−	32
$x = 0.7$	$B^4(1)$	−3.3	1.0	2.5	−	−	1.1	2
	$B^4(2)$	0.0	1.0	2.6	−	−	1.1	53
	B^3	17.5	−	−	2.6	0.2	−	45
$x = 0.8$	$B^4(2)$	0.5	1.0	2.6	−	−	0.8	48
	B^3	17.9	−	−	2.6	0.2	−	52
$x = 0.9$	$B^4(2)$	0.9	1.0	2.6	−	−	0.3	45
	B^3	18.3	−	−	2.6	0.2	−	55
$x = 1.0$	$B^4(2)$	1.3	1.0	2.6	−	−	0.0	44
	B^2	18.3	−	−	2.5	0.6		
	B^3	18.8	−	−	2.6	0.2	−	56

[a]Listed are the isotropic chemical shifts δ_{CS}^{iso}, the Gauss/Lorentz ratio G/L of the line broadening function, the line broadening parameter LB, the nuclear electric quadrupolar coupling constant C_Q, the asymmetry parameter η_Q, and the number m of B−O−P connectivities per B^4 units based on the chemical shift value and the fractional area. [b]Gauss/Lorentz character of the convolution function used: G/L = 1.0 denotes purely Gaussian broadening; G/L = 0.0 denotes purely Lorentzian broadening. [c]Line broadening parameter of the Gaussian convolution function used.
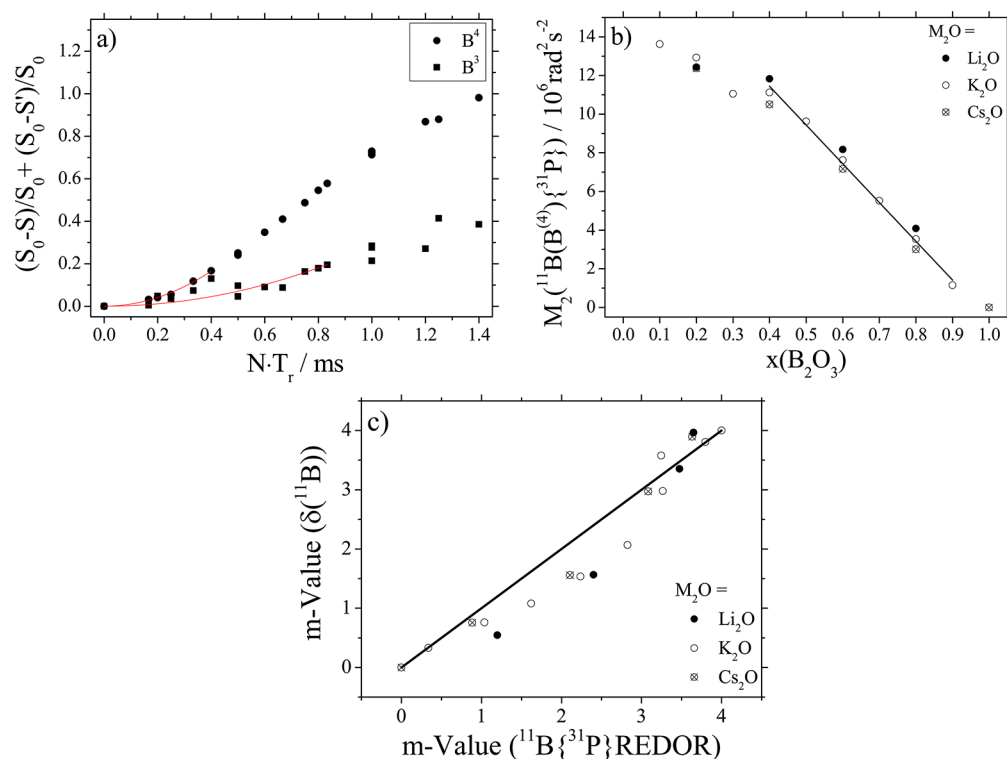
Figure 8. (a) $^{11}B\{^{31}P\}$ REDOR curve of $[K_2O]_{1/3}[(B_2O_3)_x(P_2O_5)_{1-x}]_{2/3}$ glass ($x = 0.6$). Red curves correspond to parabolic fits to eq 1, leading to the M_2 values listed in Table 4. Measurements were done at 9.4 T and MAS rotor frequencies of 8, 10, and 12 kHz. (b) M_2 values as a function of x for glasses of the systems $[M_2O]_{1/3}[(B_2O_3)_x(P_2O_5)_{1-x}]_{2/3}$ (M = Li, K, Cs). (c) Values of m determined by REDOR vs values of m determined from the ^{11}B isotropic chemical shifts for glasses of the systems $[M_2O]_{1/3}[(B_2O_3)_x(P_2O_5)_{1-x}]_{2/3}$ (M = Li, K, Cs). The solid line represents the identity case.

Table 4. $M_2(^{11}B\{^{31}P\})$ Values and m Values (in Parentheses) Based on These Measurements of Glasses in the System $[M_2O]_{1/3}[(B_2O_3)_x(P_2O_5)_{1-x}]_{2/3}$ (M = Li, K, Cs)^a

	$M_2(^{11}B^4\{^{31}P\})$ ($\pm10\%$)/10^6 rad^2 s^{-2}			$M_2(^{11}B^3)\{^{31}P\})$ ($\pm10\%$)/10^6 rad^2 s^{-2}		
	Li system	K system	Cs system	Li system	K system	Cs system
$x = 0.1$	–	13.6 (4.0)	–	–	–	–
$x = 0.2$	12.4 (3.7)	12.9 (3.8)	12.4 (3.7)	–	–	–
$x = 0.3$	–	11.1 (3.3)	–	–	–	–
$x = 0.4$	11.8 (3.5)	11.1 (3.3)	10.5 (3.1)	–	–	–
$x = 0.5$	–	9.6 (2.8)	–	–	–	–
$x = 0.6$	8.2 (2.4)	7.6 (2.2)	7.2 (2.1)	2.7	2.1	1.0
$x = 0.7$	–	5.5 (1.6)	–	–	1.1	–
$x = 0.8$	4.1 (1.2)	3.5 (1.0)	3.0 (0.9)	0.7	0.9	0.5
$x = 0.9$	–	1.2 (0.3)	–	–	0.2	–

^{a}For B^3 units, m values are assumed to be 0 (see text).

on the average ^{11}B MAS NMR shifts. Indeed, these higher values from REDOR measurements lead to a total number of B−O−P linkages that is in excellent agreement with the total number of B−O−P linkages deduced from the ^{31}P MAS NMR line shape fits (see Supporting Information, Figure S8). Altogether, the REDOR results indicate that the average number of B−O−P linkages per B^4 unit decreases slightly with increasing cation size. For the most part, this observation arises from the fact that, at a given value of x, the fraction of B$^4_{4P}$ units tends to decrease in the order Li → K → Cs as is evident from the comparison of Figure 5 and Figure S4 in the Supporting Information for $x = 0.4$ and 0.5. For the B^3 units, the average number of B−O−P linkages is always less than one in all of the glasses investigated. The REDOR effects observed here may be entirely due to spatial proximities within the third or fourth coordination spheres of boron.

High-Resolution ^{31}P MAS and Refocused INADEQUATE NMR Spectra. Figure 9 (right) shows high-speed ^{31}P MAS NMR spectra of the K-based system. While the borate-free glass, $x = 0.0$, shows a clear spectroscopic discrimination of the P^3 and the P^2 units, the resolution is substantially degraded in the boron-containing glasses, $x > 0.0$, owing to the multiple contributions arising from overlapping P$^3_{mB}$ ($0 \leq m \leq 3$) and P$^2_{mB}$ ($0 \leq m \leq 2$) units; in addition, a contribution of a P^1 species is evident only for the $x = 0.9$ sample, in agreement with the Raman spectra. Figure 9 (left) displays the double quantum filtered spectra obtained using the refocused INADEQUATE sequence. In these spectra, the line shape contributions from the isolated ^{31}P nuclei within the P$^3_{3B}$, P$^2_{2B}$, and P$^1_{1B}$ units are missing. As there are no P−O−P linkages in these units, they are not involved in any scalar ^{31}P−^{31}P spin−spin couplings, thereby precluding the buildup of double
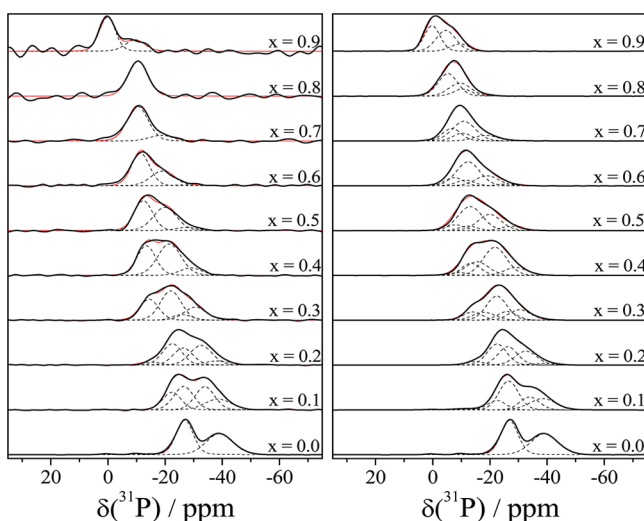
Figure 9. One-dimensional ^{31}P refocused INADEQUATE (left) and ^{31}P single pulse MAS NMR spectra (right) of glasses in the system $[K_2O]_{1/3}[(B_2O_3)_x(P_2O_5)_{1-x}]_{2/3}$, measured at 7.1 T and MAS rotor frequencies of 14.0 kHz. Spinning sidebands have been omitted for display purposes, but are included in the fits. Experimental spectra are displayed in black, their total fits are displayed in red, and the individual fitting components are shown as dashed lines. The individual components of these stack plots have been internally normalized to a constant maximum intensity and are shown with a constant vertical offset with respect to each other.

quantum coherences. Thus, particularly in glasses with higher borate contents, the number of line shape contributions to the ^{31}P NMR spectra is appreciably reduced, allowing more accurate determinations of the positions and line widths of the remaining components. Furthermore, by careful comparison of both sets of spectra, the line shape parameters of the P^3_{3B} and P^2_{2B} units can be elucidated as well. In contrast, no evidence for P^1_{1B} units is found. This is not unexpected because of the anticipated strong repulsion between the negatively charged P^1 phosphate and the anionic borate B^4 groups occurring in this composition region. However, from Figure 10 this means that the P^1 group must be a
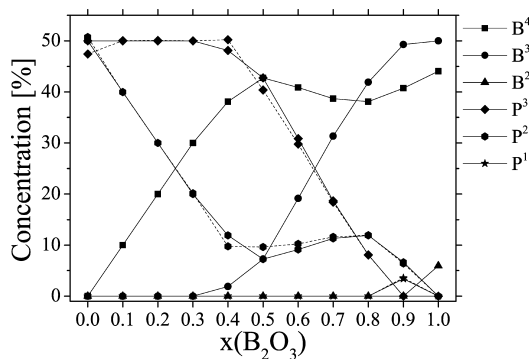

Figure 10. Network former unit species concentrations (normalized to 100%) obtained via ^{11}B MAS NMR for the B^n species and deduced for the P^n species on the basis of charge balance (solid lines) and obtained independently via deconvolution of the ^{31}P MAS NMR spectra (dashed lines), for glasses of the system $[K_2O]_{1/3}[(B_2O_3)_x(P_2O_5)_{1-x}]_{2/3}$. Lines are guides to the eye.

P^1_{1P} group, where the bonded phosphate group is a similarly charged P^2 unit. Finally, the data give no evidence for any BPO$_4$-like P^4_{4B} units in this glass system.

On the basis of this information, it is possible to constrain the fit to each of the ^{31}P MAS NMR spectra sufficiently in order to arrive at a complete line shape deconvolution into all of the possible structural species present in each of the glasses. In these fits, the respective signal intensities are the only adjustable parameters. This information is summarized in Table 5, which reveals

Table 5. Fitting Parameters of the ^{31}P MAS NMR spectra of $[K_2O]_{1/3}[(B_2O_3)_x(P_2O_5)_{1-x}]_{2/3}$ Glasses^a

	P^n_{mB}	δ_{iso} ($\pm$0.5)/ ppm	G/L^b	line width ($\pm$0.5)/ppm	area fract. ($\pm$2)/%
$x = 0.0$	P^3_{0B}	-39.0	0.9	10.9	47 (50.0)
	P^2_{0B}	-26.9	0.9	7.7	51 (50.0)
	impurity*	-9.8	0.9	5.0	1
	impurity*	0.7	0.9	7.9	1
$x = 0.1$	P^3_{0B}	-38.5	0.9	10.9	23
	P^3_{1B}	-33.9	0.9	8.0	19
	P^2_{0B}	-26.6	0.9	8.0	43
	P^3_{2B}	-22.4	0.9	7.5	13
	impurity*	-12.0	1.0	9.0	1
	impurity*	-0.2	1.0	10.3	1
$x = 0.2$	P^3_{0B}	-38.3	0.9	10.9	4
	P^3_{1B}	-32.6	0.9	9.0	26
	P^2_{0B}	-26.3	0.9	8.0	30
	P^3_{2B}	-22.5	0.9	8.0	35
	P^3_{3B}	-15.1	0.9	7.7	6
$x = 0.3$	P^3_{1B}	-30.5	0.9	9.0	19
	P^2_{0B}	-26.0	0.9	8.0	14
	P^3_{2B}	-22.4	0.9	8.5	40
	P^3_{3B}*	-18.0	0.9	9.5	15
	P^2_{1B}	-14	0.9	7.7	13
$x = 0.4$	P^3_{1B}	-29.0	0.9	9.0	12
	P^3_{2B}	-21.8	0.9	9.5	46
	P^3_{3B}*	-15.5	0.9	9.5	22
	P^2_{1B}	-13.4	0.9	7.7	16
	P^2_{2B}*	-9.5	0.9	7.5	4
$x = 0.5$	P^3_{1B}	-27.5	0.9	9.0	8
	P^3_{2B}	-19.9	0.9	9.5	30
	P^3_{3B}*	-13.1	0.9	10.0	47
	P^2_{1B}	-12.4	0.9	7.5	7
	P^2_{2B}*	-8.0	0.9	7.5	8
$x = 0.6$	P^3_{1B}	-26.5	0.9	9.0	3
	P^3_{2B}	-19.0	0.9	9.5	22
	P^3_{3B}*	-12.4	0.9	9.5	52
	P^2_{1B}	-11.4	0.9	7.5	10
	P^2_{2B}*	-7.5	0.9	7.5	14
$x = 0.7$	P^3_{2B}	-18.5	0.9	9.5	14
	P^3_{3B}*	-10.9	0.9	9.5	47
	P^2_{1B}	-10.4	0.9	7.5	15
	P^2_{2B}*	-6.7	0.9	7.5	24
$x = 0.8$	P^2_{1B}	-10.5	0.9	7.5	15
	P^3_{3B}*	-9.5	0.9	9.0	33
	P^2_{2B}*	-5.3	0.9	7.5	51
$x = 0.9$	P^2_{1B}	-9.5	0.9	7.5	15
	P^2_{2B}*	-4.6	0.9	7.5	43
	P^1_{0B}	0.2	0.9	6.5	42

^{a}Resonances not detected in the one-dimensional ^{31}P refocused INADEQUATE spectra are labeled with an asterisk. ^{b}Gauss/Lorentz character of the convolution function used: G/L = 1.0 denotes purely Gaussian broadening; G/L = 0.0 denotes purely Lorentzian broadening.

clearly that the chemical shift of each P^n_{mB} unit is not fixed all the way through the compositional series, but rather shows a monotonic

trend toward more positive values with increasing borate content, x, of the glass. This monotonic chemical shift trend arises most likely from the systematic changes encountered in the next higher connectivity spheres as the glass composition is changed in a systematic fashion.

As a validity test of the above deconvolution results, in Figure 10 we compare the total concentrations of the P^3 and P^2 units with those predicted from keeping track of the formal number of charges on the network, which must remain constant at -0.66, as a function of x. As a starting point, we may initially consider the B^4 units to be anionic species, such as they are in binary alkali borate glasses (see, however the Discussion for a more complete description of the charge distribution in these glasses as a function of x). As the concentrations of the B^4 units are easily determined from the ^{11}B MAS NMR spectra and anionic metaborate (B^2) units do not occur (except in the $x = 1.0$ glass), the fraction of phosphate units that must be present in the form of anionic metaphosphate, P^2 (and/or in the case of the $x = 0.9$ glass, pyrophosphate units, P^1, as well), can be predicted from the composition. Figure 10 indicates that the concentration of these P^2 species decreases considerably within the composition range $0 \leq x \leq 0.4$, remains essentially constant for $0.4 \leq x \leq 0.8$, and successively decreases toward 0 at the higher borate contents, $x \rightarrow 1.0$. Indeed, Figure 10 shows the excellent agreement between the species concentrations predicted from ^{11}B NMR based on such formal charge balance considerations and those obtained from the ^{31}P NMR spectral deconvolutions. Furthermore, Figure S9 in the Supporting Information illustrates that the Li- and Cs-based glasses show species concentration profiles very similar to those of the $[K_2O]_{1/3}[(B_2O_3)_x(P_2O_5)_{1-x}]_{2/3}$ glasses.

High-Resolution ^{7}Li and ^{133}Cs MAS NMR Spectra. Figure S10 in the Supporting Information shows the high-resolution ^{7}Li and ^{133}Cs NMR spectra of the Li- and Cs-based glasses. No convincing correlation was found with the quantitative contributions of the B^4 and P^2 units to the anion inventory, suggesting that it is not the nature of the charge compensating anions, borate and phosphate groups, that dominates the observed chemical shifts. Rather, the alkali ion chemical shift trends match remarkably well the compositional evolution of the ion concentration parameter N_V shown in Figure 3a. On the basis of this observation, we conclude that the cation isotropic chemical shift trends observed in these systems are dominated by ionic M···O···M interactions, the strength of which increases as the average M···M distances decrease as a function of borate content.

X-ray Photoelectron Spectra. Figure 11 shows the O 1s photoelectron spectra and their deconvolutions into the four principal environments expected, namely, oxygen within P−O−P, P−O−B, and B−O−B linkages, and P-bonded NBOs. The line shape parameters are summarized in Table 6. Despite the relatively poorly resolved spectra, excellent fitting constraints for the P−O−P, P−O$^-$ (NBO), and B−O−B units were obtained from the data for the pure potassium phosphate and the pure potassium borate glass, respectively. Line widths for the B−O−B units were found to be consistently higher than those for the other oxygen species. We attribute this to slight, but unresolvable, differences in the binding energies associated with B^3−O−B^3, B^3−O−B^4, and B^4−O−B^4 oxygen types, the signals of which are all overlapping. Keeping variations in peak positions and line widths of these contributions to a minimum, consistent line shape parameters for the P−O−B species were easily found. The peak areas of the four spectral contributions were obtained by least-squares fitting. Figure 12 illustrates that the concentration of these oxygen species are in excellent agreement with
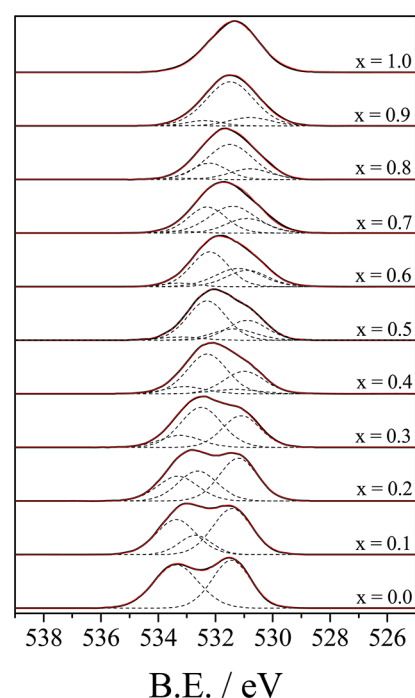

Figure 11. O 1s X-ray photoelectron spectra of glasses in the system $[K_2O]_{1/3}[(B_2O_3)_x(P_2O_5)_{1-x}]_{2/3}$ and deconvolution into four spectral components (see text). The individual components of these stack plots have been internally normalized to a constant maximum intensity and are shown with a constant vertical offset with respect to each other.

those extracted from the line shape fits of the ^{31}P MAS NMR spectra. While the structural analysis done here focuses on the O 1s spectra, K 2p and P 2p XP spectra and their line shape analyses are also reported in the Supporting Information, Figure S11 and Table S12. The K 2p electronic binding energies were found to be invariant with composition. In contrast, the P 2p binding energies show a monotonic decrease from 134.8 to 133.3 eV with increasing x. Two effects contribute to this trend: (1) the successive replacement of P−O−P by P−O−B linkages up to $x = 0.5$ and (2) the successive increase in the average number of NBO atoms bound to the P atoms in the regime $x > 0.5$. B 1s spectra could not be analyzed owing to overlap with the P 2s signals.

■ DISCUSSION

Bridging Oxygen Concentrations and Glass Transition Temperatures. The data of Figure 10 and Figure S9 in the Supporting Information provide an excellent structural rationale for the composition dependent trends observed for the T_g's of these glasses as a function of x along similar lines as previously discussed for glasses in the systems $[Na_2O]_{0.4}[(B_2O_3)_x(P_2O_5)_{1-x}]_{0.6}$[11] and $[Na_2O]_{0.35}[(B_2O_3)_x(P_2O_5)_{1-x}]_{0.65}$.[15,16] For $0.0 \leq x \leq 0.4$, the linear increase in T_g is easily explained by the fact that chain-type P^2 units are successively being replaced by three-dimensionally connected tetrahedral P^3 and B^4 units. As a result of this replacement, the average connectivity of the network increases strongly in this composition range. As a measure of this connectivity, we specify the average number of BO species per network former unit, [BO], which is available from Figure 10 and Figure S9 in the Supporting Information. As shown in Figure 13a, [BO] increases from 1.25 in the pure alkali phosphate glasses to 1.65 in the glasses with $x = 0.4$ and stays more or less constant for higher x values. Within the composition range $0.0 \leq x \leq 0.4$, the dependence of [BO] on x is universal, whereas in the region

Table 6. Binding Energies, BE, Full Width at Half-Height, Δ, and Fractional Area of the Four Distinct Oxygen Types Observed in the XPS Spectra of $[K_2O]_{1/3}[(B_2O_3)_x(P_2O_5)_{1-x}]_{2/3}$ Glasses

|	O-type	BE (±0.2)/eV	Δ(±0.2)/eV	area fract. (±5)/%
x = 0.0	NBO	531.4	1.6	51 (54.5)[a]
	P−O−P	533.4	1.8	49 (45.5)[a]
x = 0.1	NBO	531.4	1.6	47
	P−O−B	532.7	1.3	17
	P−O−P	533.4	1.7	36
x = 0.2	NBO	531.2	1.5	43
	P−O−B	532.6	1.6	31
	P−O−P	533.3	1.7	26
x = 0.3	NBO	531.1	1.5	36
	P−O−B	532.5	1.7	50
	P−O−P	533.2	1.7	15
x = 0.4	NBO	531.0	1.7	30
	B−O−B	531.3	1.9	7
	P−O−B	532.3	1.6	53
	P−O−P	533.1	1.7	10
x = 0.5	NBO	530.9	1.6	27
	B−O−B	531.4	1.9	17
	P−O−B	532.3	1.6	52
	P−O−P	533.2	1.7	5
x = 0.6	NBO	530.9	1.7	23
	B−O−B	531.2	1.9	29
	P−O−B	532.2	1.5	44
	P−O−P	533.3	1.4	4
x = 0.7	NBO	530.9	1.7	21
	B−O−B	531.4	1.9	43
	P−O−B	532.3	1.5	34
	P−O−P	533.4	1.4	2
x = 0.8	NBO	530.8	1.7	16
	B−O−B	531.5	1.9	60
	P−O−B	532.2	1.5	22
	P−O−P	533.3	1.4	2
x = 0.9	NBO	530.8	1.7	13
	B−O−B	531.5	2.0	79
	P−O−B	532.4	1.4	7
	P−O−P	533.3	1.4	1
x = 1.0	B−O−B	531.4	2.0	100

[a]Theoretically expected values.
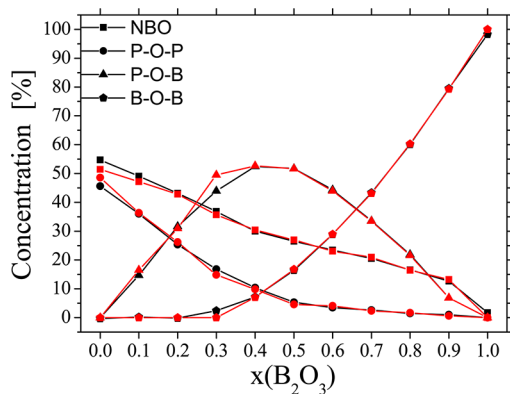
Figure 12. Oxygen speciations deduced from O 1s XPS data (red) and from the solid state NMR results (black) for glasses in the system $[K_2O]_{1/3}[(B_2O_3)_x(P_2O_5)_{1-x}]_{2/3}$.

$x > 0.4$ we can note a subtle dependence on cation type. Figure 13b illustrates the excellent linear correlations of T_g with [BO] for all
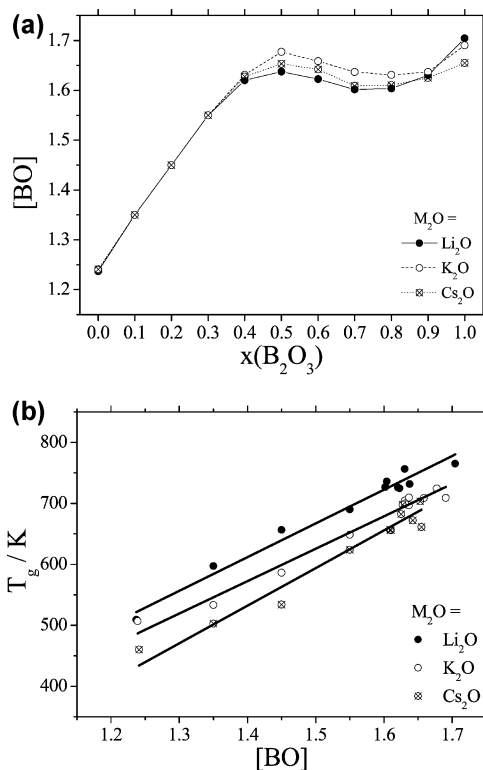

Figure 13. (a) Average number of BO species per network former unit [BO] deduced from the NMR data and (b) correlation of T_g with [BO] for glasses of the systems $[M_2O]_{1/3}[(B_2O_3)_x(P_2O_5)_{1-x}]_{2/3}$ (M = Li, K, Cs).

three systems with nearly identical slopes. Here, the cation type affects the absolute value of T_g, but not its dependence on [BO]. As expected, for a given degree of connectivity ([BO] value), T_g values increase in the direction Cs → K → Li, reflecting the effect of the cationic ion potential upon the thermal stability.

Connectivity Distribution and Medium-Range Order. The data summarized in Tables 3 and 5 also allow a direct analysis regarding the distribution of heteroatomic versus homoatomic linkages. Figure 14 compares the concentrations of
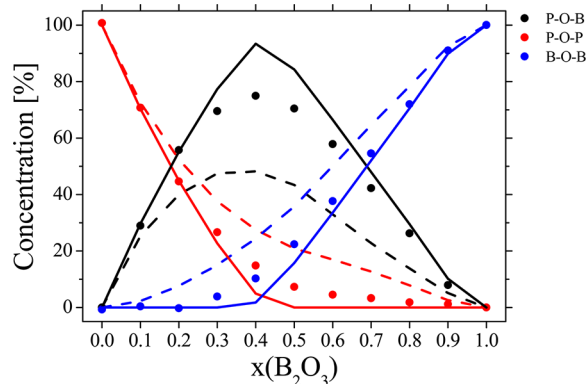

Figure 14. Connectivity distribution of the BO atoms in $[K_2O]_{1/3}$-$[(B_2O_3)_x(P_2O_5)_{1-x}]_{2/3}$ glasses derived from NMR data and comparison with different linkage scenarios. Dashed curves, random linkage scenario; solid curves, scenario corresponding to the maximum possible number of B^4-O-P linkages excluding the formation of B^3-O-P linkages.

P−O−P, B−O−P, and B−O−B linkages with two distinct structural scenarios. The dashed curves in Figure 14 represent the distribution

according to a random linkage scenario. The simulations for this scenario are based on the experimental P^n and B^n species concentrations as determined in the present study (Figure 10) and apply simple statistical (binomial) predictions. Comparisons to the experimental data illustrate that the random linkage model is clearly not applicable here. Rather, heteroatomic P–O–B connectivities are strongly preferred over homoatomic P–O–P and B–O–B linkages, despite the fact as discussed above that no B^3–O–P linkages appear to exist in these glasses. Alternatively, the solid lines in Figure 14 show the predicted numbers of B–O–P linkages under the assumption that no B^3–O–P linkages occur and the number of B^4–O–P linkages always corresponds to the maximum number possible based on the composition. This scenario is in excellent agreement with the experimental data. Therefore, we can conclude that B^4–O–P linkages, particularly those of the B^4–O–P^3 type, have special stability and are thus preferentially formed.

This special stability can be understood in terms of bond valence (BV) arguments where the charge deficit present on the $BO_{4/2}^-$ units, BV = 0.75, is balanced by the charge excess present in the P^3 units, BV = 1.25. Thus, the formation of linkages of this particular type may be considered as a major driving force controlling the structural organization of these glasses. In contrast, B^4–O–B^4 linkages are electrostatically less favorable and indeed the crystallography of alkali borates and borophosphates shows that no more than one such linkage per B^4 unit can be accommodated easily.[33] As a consequence, at borate concentrations corresponding to $x \leq 0.3$, B^4_{4P} and B^4_{3P} units dominate. For $x > 0.3$, however, the phosphorus content of the glass is no longer sufficient for the exclusive formation of these species, and hence, the formation of B^4_{mP} ($m < 3$) units becomes a necessity. These species are characterized by less negative ^{11}B chemical shifts and therefore glasses with $x = 0.4$ and 0.5 show distinct resonances for both types of B^4 species—those with $m \geq 3$ near -3 to -4 ppm and those with $m < 3$ near -1.5 to -0.5 ppm. Along with these species, trigonal boron atoms are formed to avoid the electrostatically unfavorable B^4–O–B^4 linkages, resulting in a decrease of P–O–B network connectivities. As previously suggested by us[11,18] and recently proven by two-dimensional ^{11}B dipolar correlation spectroscopy,[20] these units can be stabilized by forming B^3–O–B^4 linkages. For the same reason (electrostatic repulsion) P^1–O–B^4 linkages are unfavorable and are not detected in our NMR experiments.

Competition of the Network formers B_2O_3 and P_2O_5 for the Network Modifier and Relation to Ionic Conductivities. Based upon the borate and phosphate speciations (Figure 10), we can now quantify the competition of the two network formers B_2O_3 and P_2O_5 for the network modifier species. Each unit of M_2O added to the glassy borophosphate network creates two negative charges there, and the relative distribution of these negative charges on boron versus phosphorus could be extracted from Tables 3 and 4 if one assumes that all of the B^4 and P^2 units carry a single negative charge, whereas the P^3 and B^3 units are electrostatically neutral. In this case, the percentage of the total number of negative charges imparted on the borate network would be given by

$$[Q_B] = 2N_4x + 2N_2x \tag{2a}$$

where N_2 denotes the fraction of B^2 units, which contribute, however, only to the structure of the phosphate-free glasses. The percentage of the total number of negative charges on the phosphate network would likewise be given by

$$[Q_P] = 2([P^2] + 2[P^1]) = 2[f(P^2) + 2f(P^1)](1 - x) \tag{2b}$$

In expression 2b, the $f(P^n)$ denote the respective fractional contribution of the P^n species toward the total phosphate inventory. In the present glasses, the simplified analysis expressed by eqs 2a and 2b is, however, incorrect as it disregards the real charge distribution within the B^4–O–P^3 connectivities, which according to the results of this study dominate the glass structure over much of the compositional region. To illustrate this point, we consider a simple structural scenario for a glass with $x = 0.25$ (P/B = 3:1). For such a glass, one can construct a hypothetical network consisting mostly of P^3_{1B} and B^4_{4P} units, maximizing the number of P–O–B linkages and being consistent with the spectroscopic evidence presented in this compositional range (see Figure 15, top). In this scenario, each
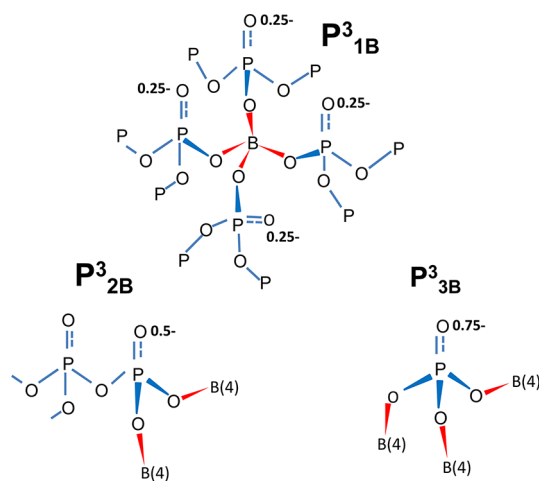

Figure 15. Charge redistribution occurring in alkali borophosphate glasses following bond valence considerations. Blue and red arrows symbolize corresponding electron distributions within P–O and B–O single bonds associated with P–O–B linkages. Top: In B^4_{4P} units linked to four P^3_{1B} units, the negative formal charge on B^4 is delocalized on the NBOs of each P^3 unit, giving each a charge of 0.25. Bottom: Analogous considerations show negative charges of 0.5 and 0.75 on the NBOs of P^3_{2B} and P^3_{3B} units, respectively.

boron contributes 3/4 valence units (vu) to each of its four B–O–P bonds while each of these four phosphorus atoms contributes 5/4 vu to its one P–O–B bond and 4/4 vu to its two P–O–P bonds, leaving 7/4 vu for its NBO. Hence, this NBO needs to be associated with a shared alkali ion to satisfy its charge requirements. In this model, the oxygens associated with the B^4_{4P} units are fully satisfied and no excess negative charge needs to be associated with them. Instead, these considerations suggest that an anionic charge of 0.25 is associated with each of the NBO atoms of these P^3_{1B} units connected to the one B^4_{4P} unit. Similar considerations suggest charges of 0.5 and 0.75 unit for P^3_{2B} and P^3_{3B} units (see Figure 15, bottom). Experimental evidence for this model comes from the Raman spectra which show that the vibrational frequency of the P–O bond associated with the P^3 sites continuously shifts toward lower values with increasing borate content (increasing x), suggesting that these oxygen atoms are no longer fully double bonded but rather assume anionic characteristics, similar to the situation present in pure alkali ultraphosphate glasses.[34] The charge distribution model presented here is also more consistent with analogous bond valence (BV) analyses of crystalline alkali borophosphates, such as $Na_5B_2P_3O_{13}$, which also show no anionic charge associated with the B^4 atoms present.[35] Finally, no crystallographic precedent exists for alkali borophosphates in which P^3 units are fully double bonded.[36]

Unfortunately, as discussed above, the relative Raman scattering intensity cross section of the borate structural groups is much less than that of the phosphate structural groups. Therefore in the low x glasses, $x < 0.4$, where these neutral B^4_{4P} groups are proposed to form, we see no Raman spectral evidence for them. It might be expected that their reduced BV of 0.75, compared to the value of 1.0 for the fully negative B^4_{4B} group, would cause this structural group to lie at a lower frequency than the 1130 cm^{-1} seen in the pure borate glasses. However, the intense modes from the P^2 phosphate groups dominate the spectral intensity in this region. While the vibrational modes in the IR spectra arising from the borate structural groups are comparable in intensity to those from the phosphate structural groups, the bands are so broad that resolution of the distinct mode assignable to the asymmetric stretch of the B^4_{4P} group at 935 cm^{-1} as seen in pure BPO$_4$[37] is not easily discernible in the IR absorption spectra of the low x glasses. However, on close inspection, there does appear to be a weak peak maximum in the IR spectra in the region of 935 cm^{-1} for the $x = 0.3$ glass, where the concentration of the B^4_{4P} groups would be expected to maximize. In the binary alkali borate glasses, the asymmetric stretch arising from B^4 groups is at ~1000 cm^{-1}, with the Li glasses having a slightly higher frequency than this and the Cs glasses having a slightly lower frequency.[38] These observations appear to support the suggestion here that the B^4_{4P} group has a smaller BV count, 0.75, than the B^4 group in pure borate glasses, 1.0.

From the above considerations, we may conclude that up to $x = 0.3$ all of the boron species present in the network can be considered electrically neutral and the anionic charge compensation is entirely provided by the phosphate network. The anionic species neutralizing the cationic charge comprise the regular anionic P^2 and the newly proposed anionic $(P^3)^{0.25-}$ species that is generated by links to B^4_{4P} units (see Figure 15). Above $x = 0.3$ new types of B^4 species appear in the ^{11}B MAS NMR spectra. Their extent of B−O−P connectivity is increasingly diminished, as increasingly B^4−O−B^3 linkages are being formed. This is reflected by the decreasing m value, extracted either from the weighted average of the ^{11}B chemical shifts of the B^4 species (Table 3, Figure 6b) or from the ^{11}B{^{31}P} REDOR data (Figure 8c). As the value m for these B^4 species decreases from 4 to 0 with increasing B content, the anionic charge on these units increases from 0 to 1. Therefore, we can approximate the average amount of charge attracted by the borate network in the borophosphate glasses using the simple formula

$$[Q_B] = 2N_4 x(4 - m)/4 + 2N_2 x \qquad (3)$$

Figure 16 summarizes the Q_B values for these glass systems, based on the $[B^4]$ and m values given in Table 3 and Tables S5 and S6 in the Supporting Information, for the K, Li, and Cs glasses, respectively. The data indicate that the phosphate network is preferentially modified over the entire composition range, providing 100% charge compensation within $0 \leq x \leq 0.3$. Borate species participate in the charge compensation only at $x \geq 0.4$ where the first B^4_{mP}, $m < 4$, groups begin to form, and their level of participation is consistently lower than predicted on the basis of the proportional sharing model.

On the basis of this analysis, we can then rationalize the compositional trends in the ionic conductivities and activation energies as displayed in Figure 3b,c. Within the compositional region $0 \leq x \leq 0.4$ the principal compositional change involves the type of phosphate unit neutralizing the cations: the anionic P^2 units initially present in the binary alkali phosphate glasses are successively replaced by the partially anionic P^3 units discussed
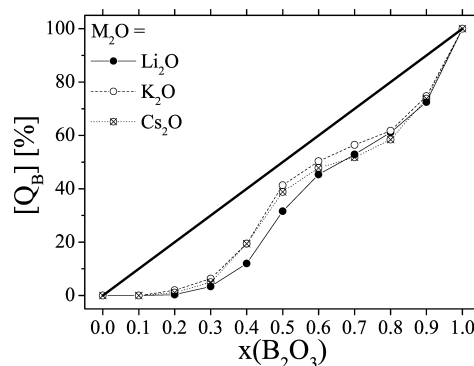

Figure 16. Percentages of the negative charge localized on the borate species as a function of x for glasses of the systems $[M_2O]_{1/3}[(B_2O_3)_x(P_2O_5)_{1-x}]_{2/3}$ (M = Li, K, Cs). Thin solid, dashed, and dotted lines are guides to the eye. The thick solid line corresponds to the scenario of proportional sharing of the modifier ion between the borate and the phosphate networks.

above. As each alkali ion must contribute only 1/4 vu to the NBO of such an anionic P^3 site, it appears plausible that they would be more weakly bound than those associated with a regular P^2 unit, where each alkali ion must contribute 2/4 vu to satisfy local charge requirements. This structural trend most likely accounts for the strong increase in the ionic conductivities (and the corresponding decrease of the activation energies) in this composition region. Above $x = 0.3$, the principal change regarding the anionic compensation involves the replacement of these anionic P^3 sites by anionic B^4 units. Again we can consider that these anionic B^4 units, in which the single charge is spread over four BOs, represent significantly shallower Coulomb traps than the anionic P^2 units and may be more comparable to those of the anionic P^3 units. These considerations explain why the ionic conductivities and activation energies do not change significantly above $x = 0.4$. Again, the cation size seems to be largely immaterial aside from determining the absolute value of the ionic conductivity measured at a given composition. Finally, the slight but discernible decrease in the conductivity and the slight increase in the conductivity activation energy for the $x = 1$ glass probably reflects the appearance of B^2 units in which the charges are not delocalized.

■ CONCLUSIONS

In summary, the present study illustrates the unique power and potential of the combined application of different solid state NMR techniques together with Raman scattering, X-ray photoelectron spectroscopy, and charge balance considerations to resolve the rather complex short- and intermediate-range-order structures of mixed network former glasses in the systems $[M_2O]_{1/3}[(B_2O_3)_x(P_2O_5)_{1-x}]_{2/3}$, M = Li, K, Cs, in a detailed and quantitative manner. The concentrations of the P$^n_{mB}$ and B$^n_{mP}$ structural units have been determined, and the overall extent of homoatomic versus heteroatomic connectivity has been quantified. The short- and medium-range-order glass structures indicate a clear preference for the formation of heteroatomic P−O−B connectivities, suggesting in particular that B^4−O−P^3 units have special stability. With the help of the structural speciations summarized in Tables 3 and 5, the compositional evolution of the macroscopic physical properties with x is easily rationalized: the dependence of T_g on x reflects the network connectivity or bond density, as expressed by the average number of BO atoms per network former species, whereas the ionic conductivity is proportional to the relative contributions of both B^4-bonded anionic

P[3] species and B[3]-bonded anionic B[4] species to the network. Both of these anionic species present extensive charge dispersion, resulting in shallower Coulomb traps than present in binary alkali phosphate glasses. Changing the network modifier type from Li to Cs produces only subtle structural variations, indicating the generalizability of the above conclusions.

■ ASSOCIATED CONTENT

Ⓢ Supporting Information

Batch compositions and those determined experimentally via EDS, Raman spectra of $[M_2O]_{1/3}[(B_2O_3)_x(P_2O_5)_{1-x}]_{2/3}$ (M = Li, Cs) glasses, FT-IR spectra of $[M_2O]_{1/3}[(B_2O_3)_x(P_2O_5)_{1-x}]_{2/3}$ (M = Li, Cs) glasses, ^{11}B MAS NMR spectra of $[M_2O]_{1/3}[(B_2O_3)_x(P_2O_5)_{1-x}]_{2/3}$ (M = Li, Cs) glasses, deconvolution of the ^{11}B MAS NMR spectra of glasses in the system $[Li_2O]_{1/3}[(B_2O_3)_x(P_2O_5)_{1-x}]_{2/3}$, deconvolution of the ^{11}B MAS NMR spectra of glasses in the system $[Cs_2O]_{1/3}[(B_2O_3)_x(P_2O_5)_{1-x}]_{2/3}$, ^{11}B TQMAS NMR spectra of representative glasses in the system $[K_2O]_{1/3}[(B_2O_3)_x(P_2O_5)_{1-x}]_{2/3}$, normalized number of B−O−P linkages present in glasses in the system $[M_2O]_{1/3}[(B_2O_3)_x(P_2O_5)_{1-x}]_{2/3}$ (M = Li, K, Cs), network former unit species concentrations in $[M_2O]_{1/3}[(B_2O_3)_x(P_2O_5)_{1-x}]_{2/3}$ (M = Li, Cs) glasses, central Zeeman transition ^{7}Li and ^{133}Cs MAS NMR spectra and isotropic chemical shifts of $[M_2O]_{1/3}[(B_2O_3)_x(P_2O_5)_{1-x}]_{2/3}$ (M = Li, Cs) glasses, K 2p and P 2p XP spectra of $[K_2O]_{1/3}[(B_2O_3)_x(P_2O_5)_{1-x}]_{2/3}$ glasses, binding energies of the K $2p_{1/2}$, K $2p_{3/2}$ and P 2p photoelectrons in $[K_2O]_{1/3}[(B_2O_3)_x(P_2O_5)_{1-x}]_{2/3}$ glasses. This material is available free of charge via the Internet at http://pubs.acs.org.

■ AUTHOR INFORMATION

Notes

The authors declare no competing financial interest.

■ ACKNOWLEDGMENTS

■ REFERENCES

(1) Levasseur, A.; Olaczuaga, R.; Kbala, M.; Zahir, M.; Hagenmuller, P.; Couzi, M. *Solid State Ionics* **1981**, *2*, 205−213.
(2) Costantini, A.; Buri, A.; Branda, F. *Solid State Ionics* **1994**, *67*, 175−178.
(3) Branda, F.; Costantini, A.; Fresa, R.; Buri, A. *Phys. Chem. Glasses* **1995**, *36*, 272−274.
(4) Takebe, H.; Harada, T.; Kuwabara, M. *J. Non-Cryst. Solids* **2006**, *352*, 709−713.
(5) Ahassou, A. P.; Rogez, J.; Kone, A. *Thermochim. Acta* **2006**, *441*, 96−100.
(6) Videau, J. J.; Ducel, J. F.; Suh, K. S.; Senegas, J. *J. Alloys Compd.* **1992**, *188*, 157−160.
(7) Ducel, J. F.; Videau, J. *J. Mater. Lett.* **1992**, *13*, 271−274.
(8) Kumar, S.; Vinatier, P.; Levasseur, A.; Rao, K. J. *J. Solid State Chem.* **2004**, *177*, 1723−1737.
(9) Anantha, P. S.; Hariharan, K. *Mater. Chem. Phys.* **2005**, *89*, 428−437.
(10) Christensen, R.; Byer, J.; Kaufmann, T.; Martin, S. W. *Phys. Chem. Glasses: Eur. J. Glass Sci. Technol., Part B* **2009**, *50*, 237−242.
(11) Zielniok, D.; Cramer, C.; Eckert, H. *Chem. Mater.* **2007**, *19*, 3162−3170.
(12) Zielniok, D.; Eckert, H.; Cramer, C. *Phys. Rev. Lett.* **2008**, *100*, 035901.
(13) Raskar, D.; Rinke, M. T.; Eckert, H. *J. Phys. Chem. C* **2008**, *112*, 12530−12539.
(14) Rinke, M. T.; Eckert, H. *Phys. Chem. Chem. Phys.* **2011**, *13*, 6552−6565.
(15) Christensen, R.; Byer, J.; Olsen, G.; Martin, S. W.; Shu, X. *Bull. Am. Ceram. Soc* **2011**, *90*, 19−22.
(16) Christensen, R.; Byer, J.; Olson, G.; Martin, S. W. *J. Non-Cryst. Solids* **2012**, *358*, 826−831. Christensen, R.; Byer, J.; Olson, G.; Martin, S. W. *J. Non-Cryst. Solids* **2012**, *358*, 583−589.
(17) Lim, J. W.; Schmitt, M. L.; Brow, R. K.; Yung, S. W. *J. Non-Cryst. Solids* **2010**, *356*, 1379−1384.
(18) Elbers, S.; Strojek, W.; Koudelka, L.; Eckert, H. *Solid State Nucl. Magn. Reson.* **2005**, *27*, 65−76.
(19) Vosejpkova, K.; Koudelka, L.; Cernosek, Z.; Mosner, P.; Montagne, L.; Revel, B. *J. Phys. Chem. Solids* **2012**, *73*, 324−329. Mosner, P.; Vosejpkova, K.; Koudelka, L.; Montagne, L.; Revel, B. *Mater. Chem. Phys.* **2010**, *124*, 732−737.
(20) Raguenet, B.; Tricot, G.; Silly, G.; Ribes, M.; Pradel, A. *J. Mater. Chem.* **2011**, *21*, 17693−17704. Raguenet, B.; Tricot, G.; Silly, G.; Ribes, M.; Pradel, A. *Solid State Ionics* **2012**, *208*, 25−30.
(21) Schuch, M.; Christensen, R.; Trott, C.; Maass, P.; Martin, S. W. *J. Phys. Chem. C* **2012**, *116*, 1503−1511.
(22) Massiot, D.; Fayon, F.; Capron, M.; King, I.; Calve, S. L.; Alonso, B.; Durand, J. O.; Bujoli, B.; Gan, Z.; Hoatson, G. *Magn. Reson. Chem.* **2002**, *40*, 70−76.
(23) Lesage, A.; Bardet, M.; Emsley, L. *J. Am. Chem. Soc.* **1999**, *121*, 10987−10993.
(24) Gullion, T.; Schaefer, J. *J. Magn. Reson.* **1989**, *81*, 196−200.
(25) Bertmer, M.; Eckert, H. *Solid State Nucl. Magn. Reson.* **1999**, *15*, 139−152.
(26) Chan, J. C. C.; Eckert, H. *J. Magn. Reson.* **2000**, *147*, 170−178.
(27) Gullion, T. *Magn. Reson. Rev.* **1997**, *17*, 83−131.
(28) Strojek, W.; Fehse, C. M.; Eckert, H.; Ewald, B.; Kniep, R. *Solid State Nucl. Magn. Reson.* **2007**, *32*, 89−98.
(29) Yao, W.; Martin, S. W. *Solid State Ionics* **2008**, *178*, 1777−1784.
(30) Hudgens, J. J.; Brow, R. K.; Tallant, D. R.; Martin, S. W. *J. Non-Cryst. Solids* **1998**, *223*, 21−31.
(31) Bril, T. W. *Philips Res. Rep., Suppl.* **1976**, *2*, 1−114.
(32) Konijendijk, W. L.; Stevels, J. M. *J. Non-Cryst. Solids* **1975**, *18*, 307−331.
(33) Wright, A. C. *Phys. Chem. Glasses: Eur. J. Glass Sci. Technol., Part B* **2010**, *51*, 1−39.
(34) Hoppe, U. *J. Non-Cryst. Solids* **1996**, *195*, 138−147.
(35) Ewald, B.; Kniep, R. *Inorg. Chem.* **2005**, *44*, 6431−6438.
(36) Kniep, R.; Engelhard, H.; Hauf, C. *Chem. Mater.* **1998**, *10*, 2930−2934.
(37) Adamczyk, A.; Handke, M. *J. Mol. Struct.* **2000**, *555*, 159−164.
(38) Verhoef, A. H.; den Hartog, H. W. *J. Non-Cryst. Solids* **1995**, *182*, 221−234.